UAB Universitat Autònoma de Barcelona
Facultat de Ciències

Treball Final de Grau en Física

Studying radiative transfer in the evolving atmosphere of lava planet K2-141b

Gunnar Montseny Gens

Tutor acadèmic: Dr. T. Giang Nguyen

Tutor administratiu: Dr. Lluís Font Guiteras

Curs acadèmic: 2024-2025

Convocatòria: Juliol 2025

DECLARACIÓ D'AUTORIA DEL TREBALL DE GRAU

Jo, Gunnar Montseny Gens, amb Document Nacional de Identitat 54760720C, i estudiant del Grau en Física de la Universitat Autònoma de Barcelona, en relació amb la memòria del treball de final de Grau presentada pera a la seva defensa i avaluació durant la convocatòria de Juliol del curs 2024-2025, declara que:

- El document presentat és original i ha estat realitzat per la seva persona.
- El treball s'ha dut a terme principalment amb l'objectiu d'avaluar l'assignatura de treball de grau en física en la UAB, i no s'ha presentat prèviament per ser qualificat en l'avaluació de cap altre assignatura ni aquesta ni en cap altre universitat.
- En el cas de continguts de treballs publicat per terceres persones, l'autoria està clarament atribuïda, citant les fonts degudament.
- En el casos en els que el meu treball s'ha realitzat en col·laboració amb altres investigador i/o estudiants, es declara amb exactitud quines contribucions es deriven del treball de tercers i quines es deriven de la meva contribució.
- A l'excepció del punts esmentat anteriorment, el treball presentat és de la meva autoria.

Signatura:

GUNNAR MONTSENY GENS - DNI 54760720C

Digitally signed by GUNNAR MONTSENY GENS - DNI 54760720C
Date: 2025.06.13 23:38:35 +02'00'

DECLARACIÓ D'EXTENSIÓ DEL TREBALL DE GRAU

Jo, Gunnar Montseny Gens, amb Document Nacional de Identitat 54760720C, i estudiant del Grau en Física de la Universitat Autònoma de Barcelona, en relació amb la memòria del treball de final de Grau presentada pera a la seva defensa i avaluació durant la convocatòria de Juliol del curs 2024-2025, declara que:

- El nombre total de paraules (segons comptatge proposat [1]) incloses en les seccions des de la introducció a les conclusions és de 8322 paraules.
- El nombre total de figures és de 7.

En total, el document comptabilitza:

$$8322 \text{ paraules} + 7 \times 200 \text{ paraules/figura} = 9722 \text{ paraules}$$

Que compleix amb la normativa al ser inferior a 10000.

Signatura:

GUNNAR MONTSENY GENS - DNI 54760720C

Digitally signed by GUNNAR MONTSENY GENS - DNI 54760720C
Date: 2025.06.13 23:39:25 +02'00'

[1] Utilitza l'eina de comptatge de paraules de Word. La versió Word 365, amb llicència de campus UAB, permet obrir arxius pdf. Per tal de fer el comptatge s'ha de seleccionar el text des de la introducció fins a les conclusions. Queden exclosos del comptatge: abstract, referències, annexos i qualsevol document que no formi part pròpiament del cos del treball.

Abstract

Lava planets are rocky exoplanets with surface temperatures high enough to sustain a magma ocean and a vaporized silicate-rich atmosphere. They orbit extremely close to their host star, leading to tidal locking, which creates a hot permanent dayside and a cold permanent nightside. Studying these lava worlds provides unique opportunities to explore planetary formation, magma ocean dynamics, and early evolutionary stages of rocky planets.

This thesis studies the radiative transfer in the atmosphere of lava planet K2-141b at different evolutionary stages. A Python framework was developed to calculate total opacity and absorbed stellar and surface flux for any given magma ocean composition. The results indicate that changes in magma ocean composition do not significantly affect K2-141b's atmosphere, but variations in geothermal flux cause substantial differences in surface temperatures. In its early stage, when K2-141b's mantle is fully molten and hosts a global magma ocean, the atmosphere is denser, optically thicker, and more extended. On the other hand, the late stage of K2-141b only has a shallow magma ocean on the dayside, leading to an optically thinner and more localized atmosphere. As a result, the total absorbed flux by the atmosphere is higher in the early stage than in the late stage.

The results and computational tools developed in this thesis will contribute to ongoing efforts to build a coupled radiative transfer and hydrodynamical model for exoplanet atmospheres. This model, currently being developed by my supervisor Dr. Nguyen and other collaborators, aims to fully characterize lava planet atmospheres when observational data from JWST becomes available.

Contents

Acronyms

BSE Bulk Silicate Earth. 10

CMB Core-Mantle Boundary. 9

GMO Global Magma Ocean. 9, 10, 14, 16, 17

JWST James Webb Space Telescope. 3, 7, 15, 18, 24

MMO 'Mushy' Magma Ocean. 10

SMO Shallow Magma Ocean. 9, 10, 14, 16, 17

1 Introduction

1.1 Motivation for studying lava planets

Exoplanets are planets that orbit stars outside of our Solar System. Although more than 5500 have been detected to date, current estimates suggest that only a small fraction of the total population has been discovered (Kaushik, Mattoo, and Rastogi 2024). Studying these distant worlds allows us to deepen our understanding of planetary formation and evolution, assess their potential habitability, and search for signs of life beyond Earth.

Among them, lava planets stand out as particularly interesting targets. They are defined as terrestrial exoplanets with predominantly rocky compositions (dominated by silicates and metals) and surface temperatures high enough to allow silicate melting (Nguyen, Cowan, Pierrehumbert, et al. 2022). As a result, they can potentially support magma oceans and develop a vaporized silicate rock atmosphere (Buchem et al. 2023). To date, more than 500 rocky exoplanets orbiting their host star with an orbital period smaller than 10 days have been detected (Zilinskas et al. 2022), making them strong candidates for classification as lava planets, as their predicted substellar equilibrium temperatures range between 1500 K and 4000 K.

Notably, the atmosphere of lava planets is strongly coupled to their interior. Since the expected silicate-rich atmospheres of lava planets are generated by magma ocean outgassing processes, observing them could help us understand the planets' interior dynamics, composition, formation and evolution. This strong relationship between atmosphere and planet interior offers a unique opportunity to study geological processes not seen anywhere else.

Another key characteristic of lava planets is their extreme climate caused by tidal locking, making them valuable targets for atmospheric studies. Lava planets are tidally locked into synchronous rotation around their host star, meaning they have a permanent hot dayside and a permanent cold nightside. Surface temperatures on the dayside are high enough to melt silicate rock and create a vaporized silicate rock atmosphere. Since the outgassing processes are temperature-dependent, big temperature differences between the dayside and the nightside lead to considerable vapor pressure differences, causing a pressure gradient that maintains horizontal flow (Nguyen, Cowan, Banerjee, et al. 2020). However, according to current theoretical models (Nguyen, Cowan, and Dang 2024), the atmosphere might collapse before reaching the nightside through rock rain. Consequently, relatively matured lava planets likely host a non-global condensing atmosphere restricted to part of the dayside.

From an evolutionary perspective, lava planets could offer insight into early stages of planetary formation. Boukaré et al. 2023 predicts that they start with a deep magma ocean, likely encompassing all of the planet's mantle. Due to the extreme proximity to their host stars, the enormous amount of stellar flux absorbed by the planet on its dayside is enough to keep at least a shallow magma ocean on the dayside throughout its evolution, not allowing it to form a stable and solid planet-wide crust. Planetesimals and rocky planets formed through accretion likely had a magma ocean in their early evolutionary stages but eventually cooled down and formed a stable and solid planet-wide crust (Schaefer and Elkins-Tanton 2018). Unlike typical rocky planets, lava worlds can sustain a surface lava ocean for longer and extend this unusual evolutionary stage. Consequently, they present a unique opportunity to explore the formation and early stages of rocky planets, including those found in our own Solar System.

1.2 Observational background and selection of K2-141b

Lava worlds are ideal candidates for extensive observations because they offer relatively high signal-to-noise ratios, and could host the first unambiguous atmospheric detection on a rocky planet outside the Solar System. Some of them have been observed with all types of telescopes. However, results have not been decisive and definitive scientific proof of an atmosphere has noot been found. As of now, theoretical models and currently limited observations by K2 (2018) and Spitzer (2019) predict a very physically thin atmosphere or no atmosphere at all on K2-141b (Zieba et al. 2022). Note that K2-141b is the lava planet with the highest signal-to-noise ratio ever detected, hence the decision to select it as our object of study (Nguyen, Cowan, Banerjee, et al. 2020). Table 1 displays important K2-141b properties:

Table 1: K2-141b (Malavolta et al. 2018)

Mass M_p	$5,08 \pm 0,41\ M_\oplus$
Radius R_p	$1,51 \pm 0,05\ R_\oplus$
Distance to host star d (AU)	$(7,47 \pm 0,10) \cdot 10^{-3}$
Orbital period T_p (Earth days)	$0,2803244 \pm 0,0000015$
Surface gravity g_p	$(2,23 \pm 0,33)g$
Eccentricity e_p	0

$M_\oplus = 5,97 \cdot 10^{24}$ kg, $R_\oplus = 6371$ km, and $g = 9,81$ m/s^2.

Newer telescopes like JWST may make it possible to definitely detect an atmosphere and further characterize it through extensive observation campaigns. So far, 12 lava planets have been selected for JWST observations, with two of them having already been observed in the General Observers program Cycle 1 (K2-141b and 55 Cancri e). However, public data for these observations has not yet been released.

1.3 Objectives and hypothesis

Planet K2-141b was discovered in 2018 (Malavolta et al. 2018), and since then, several universities have analyzed observational data and have developed theoretical models. Hydrodynamical models and radiative transfer models were developed separately, both delivering interesting predictions but without completeness and full of assumptions. Hydrodynamical models used pure atmospheres of SiO, Na, and O_2, whereas radiative transfer models were chemically complex but neglected atmospheric flow and its consequences. In 2022, the first work to couple radiative transfer and hydrodynamics was done by Dr. Nguyen (Nguyen, Cowan, Pierrehumbert, et al. 2022). Currently, a more extensive numerical model is being developed combining hydrodynamics, radiative transfer, melt-vapor equilibrium, and interior dynamics. I was fortunate enough to cross paths with Dr. Nguyen at McGill University in Montréal, allowing me to enter this project and work on the radiative transfer part.

This thesis aims to study radiative transfer in different evolutionary stages of a lava planet, coupling the dynamics between a chemically-complex atmosphere and its underlying magma ocean. The evolution of magma ocean composition, ocean dynamics, and surface temperature may affect atmospheric opacity, leading to significant changes in radiative transfer, atmospheric dynamics, and observability conditions (Boukaré et al. 2023).

The magma ocean model detailed in (Boukaré et al. 2023) provides the magma ocean composition over time. Then, LavAtmos (see Section 3.1) is used (Buchem et al. 2023) to determine which materials are sublimated/evaporated, and their abundance in the atmosphere above assuming thermochemical equilibrium. These first two steps were facilitated by Dr. Nguyen, resulting in data files containing partial vapor pressure values as a function of surface temperature and magma ocean composition.

Based on these input files, the first objective of this thesis is to develop a systematic approach to calculate atmospheric opacity given any atmospheric composition, using available data from ExoMol (see Section 3.2). The second objective is to calculate stellar radiation and surface blackbody radiation absorbed by the atmosphere for any given atmospheric composition. Results, as well as the Python code from this thesis will be used to aid Dr. Nguyen reduce computational time in his numerical model, and build an intuition based on new insights this thesis might offer. Finally, the third objective is to combine both developed methods and apply them to analyze how atmospheric properties and radiative transfer processes evolve between the early and late evolutionary stages of a lava planet.

The hypothesis of this thesis is that the atmosphere of K2-141b starts as an optically thick atmosphere, but as the planet cools, changes in the magma ocean composition and a reduction of ocean dynamics lead to an optically thinner atmosphere. This evolution affects the radiative transfer properties of the atmosphere, resulting in higher absorbed flux during the early stages of K2-141b.

2 Theoretical background

Let us start with some general definitions:
Substellar point: fixed location on a planet where stellar flux hits the planet's surface perpendicularly. It is where stellar flux is the highest.

Co-latitude/angular distance from substellar point θ: angle between the substellar point and any location on the planet. Possible values go from 0 to 180°. Therefore, the substellar point has coordinates (0,0) = (latitude λ_l, longitude ϕ_l) and $\theta = 0$. For any point in the surface with coordinates (λ_l,ϕ_l), the angular distance from the substellar point is:

$$\theta(\lambda_l, \phi_l) = \cos^{-1}(\cos\phi_l \cos\lambda_l). \tag{1}$$

Terminator: angular distance from the substellar point where stellar flux ceases to impact the planet's surface. In a lava planet, due to the proximity to its host star, it need not be $\theta = 90°$ (Read Section 2.5).

This section will present the necessary theoretical background to prepare the reader for the results of this thesis. It begins with general scientific context about lava planets, including their evolutionary stages and the role of volatile species in their atmosphere. Then, the focus shifts to specific assumptions, methods and calculations used in this work to analyze atmospheric radiative transfer and determine dayside surface temperatures of lava planets.

2.1 Evolutionary stages of lava planets

There are four distinct evolutionary stages described in the model developed in (Boukaré et al. 2023). The model assumes that the CMB is at $R_{CMB} = 0.7505\ R_{\oplus}$, exactly at half the radius of K2-141b, which is also assumed in this thesis. The iron core will not be considered for the interior dynamics, only the mantle.

Initially, all rocky planets (exoplanets, Earth included among others) start with deep magma oceans likely occupying the whole mantle due to the thermal consequences of planet formation (Schaefer and Elkins-Tanton 2018). This represents Stage 1, or the Global Magma Ocean (GMO) stage. However, a lava planet is extremely close to its host star, which helps to maintain a Shallow Magma Ocean (SMO) on the dayside even after billions of years. This is the final Stage 4, in which K2-141b is currently thought to be in.

As the lava planet evolves in time and cools down, its thermal history can be split into distinct evolutionary stages. Despite the huge incident stellar flux and tidal effects, lava planets cannot stay hot enough to sustain a global magma ocean. The permanent nightside receives no stellar flux, and therefore radiates away its initial heat to space and cools until blackbody emission is balanced with negligible geothermal heat. The last stage is reached when a SMO reaches an equilibrium state on the dayside. Duration for each stage depends on many external factors, but Stage 4 is predicted to be the longest (Herath et al. 2024).

- ***STAGE 1*: Global Magma Ocean (GMO)**
  There is a deep magma ocean on both sides of the lava planet, and the whole mantle is molten. Surface temperatures on the dayside can be as high as 2000 K-4000 K. On the nightside, the crust is not yet solid, and the average surface temperature is 1500 K. When surface lava on the nightside starts to solidify, it becomes denser and sinks, letting new hot magma raise, which helps maintain a high surface temperature. The surface is unstable, but the high temperatures make it radiate a lot of flux and if a

detected lava planet has nightside temperatures higher than 1000 K, it most probably is in Stage 1.

The GMO is highly homogeneous and similar to a BSE composition. Horizontal convection caused by the dayside/nightside temperature gradient and vertical convection caused by the surface replenishment helps keep it homogeneous with no stratification, chemical or solid-liquid-fractionation.

- ***STAGES 2 AND 3*: Beginning and end of the 'Mushy' Magma Ocean (MMO)**
  Solidification starts to take place. At 40% melt fraction, the mantle's behaviour is more similar to a solid than a liquid. Regions where melt fraction is between 20% and 60% are called 'mushy', in the sense that they are a mix of liquid and solid as crystallization has begun. Chemical fractionation begins, and so the mantle hosts a different mix of liquid and crystal species. As chemical fractionation continues, the magma ocean becomes more stratified.

  As stratification takes hold, convection in the mantle is reduced, and a crust in the nightside is formed and stabilized. Incompatible species (which prefer to be in a molten state rather than a solid state) like FeO, SiO, SiO_2, Na and K will try to avoid crystallization while compatible species like MgO while will most likely solidify. See Table 2 for more details.

- ***STAGE 4*: Solid interior with shallow dayside magma ocean**
  At this stage, 20% of the molten mantle is liquid on the dayside, where the surface is kept molten due to the high stellar flux. The maximum depth of the remaining magma ocean is predicted to be less than 200 km, but surface temperatures above the dayside SMO can still be around 2000-3000 K. The SMO is expected to be highly silicate-rich with negligible convection. Deeper in the dayside mantle, stratification and chemical fractionation are now complete.

  On the nightside, there is a solid and stable crust, and the mantle beneath it is solid and dynamically inactive. The nightside emission is solely balanced with geothermal heating, which is low. Therefore, the equilibrium temperature on the nightside is around 100 K.

Table 2: Melting temperatures (in K) of species in $\mathcal{A}$ (Kracek 1963)

O_2	SiO	SiO_2	AlO	TiO	MgO	CaO	Na	K
54,35	2065,15	1943,15	567,78	2023,15	3073,15	2843,15	370,97	336,55

It is important to note that the required input files for carrying out this thesis were obtained from Dr. Boukaré through Dr. Nguyen. I received two .txt files, one corresponding to the partial vapor pressures of the atmosphere above the magma ocean in Stage 1 and the other for Stage 4 (Boukaré et al. 2023). For more information, read Section 3.

2.2 Volatility

A **volatile** species is an element or a molecule that easily evaporates/sublimates for typical conditions of a planet. Na and K are examples of volatiles on lava planets. Although Na and K are less common in the mantle than silicates (Herath et al. 2024), they could potentially

be a significant contributor to the total vapor pressure because of their predisposition to transform into a gas phase. After evaporation/sublimation, Na and K are expected to be transported horizontally through the atmosphere until they condense on the cold nightside.

Theoretical models predict they will condense out farther from the substellar point than non-volatiles (Kite et al. 2016). As the lava planet evolves and the magma ocean continues to recede, volatiles increasingly condense more onto solid crust rather than magma ocean. Once they fall on the dynamically inactive crust, they cannot be recycled back to the atmosphere through magma ocean circulation, and solid flow is negligible at small scales (Nguyen, Cowan, Banerjee, et al. 2020). Therefore, volatile atmospheric constituents might deplete themselves because they evaporate/sublimate too fast and their solid return rate through the magma ocean is not fast enough to keep up. This process is called **cold-trapping**.

On the other hand, **refractory** species, also known as non-volatiles, such as SiO,CaO and MgO, tend to remain more in molten or solid state rather than gas state. They are much more abundant in the magma ocean making them contribute significantly to the atmosphere through considerable outgassing.

2.3 Model assumptions

Now that a general scientific background in lava planets has been explored, the focus can go back to the characterization of K2-141b's atmosphere. In order to compute the results for this thesis, several assumptions are needed:

1. The magma ocean and the silicate atmosphere are in chemical equilibrium: changes are initially induced in the magma ocean composition and dynamics, after which surface temperature and atmospheric radiative consequences are assessed. Chemical equilibrium implies that the saturated vapor pressures from LavAtmos can be used as surface pressures.
2. To isolate the effect of different magma ocean compositions on the atmosphere during different evolutionary stages, atmospheric escape and cold-trapping (see Section 2.2) will initially be neglected. However, these processes are expected to be common in the atmospheres of lava planets (Nguyen, Cowan, and Dang 2024) and will be incorporated later in this thesis to quantify their effect.
3. No additional non-rock volatiles such as N_2 or CO_2 are considered, as it is assumed that the condensible atmosphere is solely formed by evaporation/sublimation of lava and surface rocks.
4. Oceanic timescale is assumed to be orders of magnitudes longer than atmospheric timescale, allowing the atmosphere to reach steady state given any evolutionary stage of the magma ocean. Therefore, only co-latitude dependence is analyzed in each evolutionary stage.
5. The selected species for our model are $\mathcal{A} = \{\text{SiO, } SiO_2\text{, Na, } O_2\text{, AlO, TiO, MgO, CaO, K}\}$. The actual K2-141b atmosphere is most certainly composed of more atmospheric species, but the ones included in $\mathcal{A}$ are relevant enough in a silicate-rich atmosphere to make this thesis doable (additional reasons discussed in Section 3.2).
6. No Coriolis forces are considered to preserve axial symmetry and reduce complexities.
7. The surface of K2-141b and its star behave like perfect blackbodies (emissivity is 1 and surface albedo is 0), again for simplification purposes.

2.4 Radiative transfer formulation

First, the vertical optical depth τ_i for species $i \in \mathcal{A}$ describes how much flux is absorbed in a vertical column through the atmosphere by species i (Nguyen, Cowan, and Dang 2024):

$$\tau_i(\lambda, P_i, P_{\text{atm}}, T_{\text{atm}}) = \frac{x_i(\lambda, P_{\text{atm}}, T_{\text{atm}})P_i}{m_i g_p}, \tag{2}$$

where $x_i(\lambda, P_{\text{atm}}, T_{\text{atm}})$ is the wavelength-dependent absorption cross-section at total atmospheric pressure P_{atm} and at atmospheric temperature $T_{\mathbf{atm}}$, P_i is the partial vapor pressure of species i in the atmosphere, m_i is its molar mass of species i (see Appendix 6.1) and g_p is the gravitational acceleration on K2-141b. Absorption-cross section has units of m^2/molecule, as it represents the effective area in which atoms of species i will absorb flux (incoming photons) at different wavelengths.

With the input files given by Dr. Nguyen, I have $P_{\text{atm}}(T_{\text{surf}})$ and $P_i(T_{\text{surf}})$. Since the atmospheric analysis is being performed just above the surface, $T_{\text{surf}} \approx T_{\text{atm}}$ can be assumed (Read more in Section 3). Finally, $T_{\text{atm}}(\theta)$ can be obtained, making the optical depth only depend on wavelength λ and co-latitude θ.

The emissivity/absorptivity/opacity ϵ of atmospheric constituent i is defined as:

$$\epsilon_i(\lambda, \theta) = 1 - e^{-\tau_i(\lambda,\theta)} \in [0, 1]. \tag{3}$$

For the total opacity, all the exponents from different atmospheric species are added:

$$\epsilon_{\text{total}}(\lambda, \theta) = 1 - e^{-\sum_{i\in\mathcal{A}} \tau_i(\lambda,\theta)} \in [0, 1]. \tag{4}$$

Both optical depths and opacity are dimensionless quantities that describe how much flux is absorbed. When an atmosphere is opaque, its total optical depth satisfies $\tau >> 1$ and its total opacity is close to 1. On the other hand, a transparent atmosphere has $\epsilon \approx 0$ and $\tau << 1$. Note that $\epsilon = 0$ across all wavelengths implies that all light is being transmitted through the atmosphere without any absorption features. Although this could imply the absence of an atmosphere, it could also arise from limited observational precision.

Now that the concept of opacity has been introduced, the radiative balance of a given atmosphere is much easier to understand. Let's consider the following terms as described in (Nguyen, Cowan, and Dang 2024):

- Stellar radiation absorbed by the atmosphere:

$$F_{\text{stel}}(\theta) = \int_0^\infty \epsilon_{\text{total}}(\lambda, \theta) F_*(\theta, \lambda) d\lambda, \tag{5}$$

  where F_* is the stellar flux from the nearby star colliding with K2-141b's atmosphere. Note that the stellar flux depends on θ, explicit formulas are stated in Section 2.5 through Eqs (11) and (12).

- Surface blackbody radiation absorbed by the atmosphere:

$$F_{\text{surf}}(\theta) = \pi \int_0^\infty \epsilon_{\text{total}}(\lambda, \theta) B(T_{\text{surf}}(\theta), \lambda) d\lambda, \tag{6}$$

  where T_{surf} is the temperature of the surface and $B(T_{\text{surf}}, \lambda)$ is the Planck blackbody function (see Eq 7). Surface emissivity is assumed to be approximately 1, which is why it is not included in Eq (6). Note that the π factor is due to the integration over all solid angles.

- Planck's blackbody radiation has the following dependence with λ and T:

$$B(T,\lambda) = \frac{2hc^5}{\lambda^5}\frac{1}{e^{hc/\lambda k_B T} - 1}. \tag{7}$$

- Broadband opacity:

$$\epsilon_B(\theta) = \frac{\int_0^\infty \epsilon_{\text{total}}(\lambda,\theta)F_*(\theta,\lambda)d\lambda}{\int_0^\infty F_*(\theta,\lambda)d\lambda}. \tag{8}$$

  It is the atmospheric opacity averaged over the wavelength space and weighted by stellar flux. Intuitively, it is the ratio between stellar flux absorbed by the atmosphere and total stellar flux integrated across all wavelengths.

Atmospheric radiative cooling will not be discussed in this thesis because of the complexities arising from the specific vertical structure of the atmosphere that can only be determined in conjunction with a hydrodynamical model. Assessing radiative cooling of the atmosphere therefore exceeds the scope of this thesis.

2.5 Dayside surface temperature

In the scope of this thesis, surface temperature will be calculated through radiative equilibrium assuming that there is no atmospheric absorption in either Stage 1 or Stage 4. If atmospheric absorption of stellar flux was considered for surface temperature calculation, it would be a loop problem as stellar flux absorption depends on the atmospheric composition which in turn depends on surface temperature. A full radiative transfer and a hydrodynamics model is needed for accurate surface temperature calculations. Thus, the surface temperatures obtained for each stage will be preliminary but will offer a good approximation of how stellar flux and geothermal flux affect surface temperature.

Normally, when surface radiative equilibrium temperatures are calculated in exoplanets, it is assumed that the star is far enough from the planet, and a parallel rays approximation can be used. This way, half of the planet gets illuminated by the star, and the other half does not. Let F_{stel} be the stellar flux incident on the exoplanets' surface and F_{geo} the geothermal flux (flux flowing from the planet's interior into the surface through conduction and convection). The total flux absorbed by the exoplanet's surface is $F_{\text{abs}} = F_{\text{stel}} + F_{\text{geo}}$, and the flux emitted by the surface is $F_{\text{em}} = \sigma T_s^4$ (assuming $A_B = 0$ and $\epsilon_{\text{surf}} = 1$). In radiative equilibrium, absorbed flux must be equal to emitted flux:

$$F_{\text{abs}} = F_{\text{em}} \implies T_s = ((F_{\text{stel}} + F_{\text{geo}})/\sigma)^{1/4}. \tag{9}$$

In the case of K2-141b, the planet is too close to its host star K2-141 for the parallel rays approximation to be applied. This forces a geometrical situation where there is a region on the planet that is **fully illuminated** by the star and another that is partially illuminated, or otherwise named the **penumbra region**. In this region, part of the star is blocked by the horizon, and parallel ray approximations cannot be applied. After the penumbra region, the surface lies in permanent darkness. Let us calculate the surface radiative equilibrium temperature for each region (note that all of the following formulas can be found in Appendix A in (Kang, Nimmo, and Ding 2023)).

Let us start by calculating the co-latitude limits for these regions. The **fully illuminated region** spans from 0 to θ_f, the **penumbra region** spans from θ_f to θ_d, and the dayside of the lava planet spans from 0 to θ_d. θ_d is where the terminator is, and after this co-latitude

no stellar flux reaches the surface, making it the starting point for the nightside. Both angles are defined with the following formulas:

$$\theta_f = \arccos((R_p + R_*)/d), \qquad \theta_d = \arccos((R_p - R_*)/d), \tag{10}$$

where R_p and d can be found in Table 1 and $R_* = (0,681 \pm 0,018)R_\odot$ is the radius of host star K2-141 (Bonomo et al. 2023). Uncertainty formulas for these two angles can be found in Appendix 6.2. For K2-141b, $\theta_f = (\mathbf{64}, \mathbf{37} \pm \mathbf{0}, \mathbf{81})^\circ$ and $\theta_d = (\mathbf{114}, \mathbf{54} \pm \mathbf{0}, \mathbf{79})^\circ$.

The full geometrical calculations can be found in (Kopal 1954), but for the scope of this thesis, we only need the geometrical factor for each case:

- Fully illuminated zone ($\theta < \theta_f$):

$$T_s(\theta) = \left(\frac{F_{\text{stel},f}(\theta) + F_{\text{geo}}(\text{Stage})}{\sigma} \right)^{1/4}, \quad F_{\text{stel},f}(\theta) = \pi \int_0^\infty \epsilon_{\text{total}}(\lambda, \theta) J_f(\theta) B(\lambda, T_*) d\lambda, \tag{11}$$

  where T_s represents the surface temperature, $T_* = 4570 \pm 100$ K the effective temperature of star K2-141 (Bonomo et al. 2023), and $F_{\text{stel},f}$ the absorbed stellar flux for co-latitudes in this region. Stage-dependent F_{geo} is estimated in Section 2.5.1, and a specific formula for $J_f(\theta)$ is detailed in Appendix 6.2.

- Penumbra region ($\theta_f < \theta < \theta_d$):

$$T_s(\theta) = \left(\frac{F_{\text{stel},p}(\theta) + F_{\text{geo}}(\text{Stage})}{\sigma} \right)^{1/4}, \quad F_{\text{stel},p}(\theta) = \pi \int_0^\infty \epsilon_{\text{total}}(\lambda, \theta) J_p(\theta) B(\lambda, T_*) d\lambda, \tag{12}$$

  where T_s represents the surface temperature, and $F_{\text{stel},p}$ the absorbed stellar flux for co-latitudes in this region. A specific formula for $J_p(\theta)$ is detailed in Appendix 6.2.

2.5.1 Geothermal flux estimation

Lava planets in their Stage 1 have a GMO, consisting of a molten mantle and constant resurfacing of hot lava as denser, solidified crust gradually sinks to the bottom of the magma ocean or until it fins denser magma. Therefore, nightside temperatures are expected to have an average of 1500 K (Boukaré et al. 2023). Since there is no stellar flux on the nightside, this implies that interior heat flux is considerable and can not be neglected for Stage 1. Assuming that no stellar flux is reaching the surface in the night side, we have that at any point in this side, $\sigma T_s^4 = F_{\text{geo}}$ is true. Substituting $T_s = 1500$ K, we obtain an internal heat flux of $F_{\text{geo}} = 287043,75$ W/m^2. This value is significant due to vertical convection, and it is within the typical range of geothermal flux in lava planets during their early stages (Boukaré et al. 2023). As the GMO is homogenized at this stage, the same amount of internal heat flux will be assumed for the whole planet.

However, for Stage 4, temperatures in the nightside are expected to cool to 100 K, making internal heating almost irrelevant with $F_{\text{geo}} = 5.67$ W/m^2. Here, the crust on the nightside has solidified and radiates as much flux as internal heating. We set the geothermal flux as this value for the entire planet in Stage 4. The assumption is justified because of the small magma ocean depth 200 km (Boukaré et al. 2023), which ends up being less than 5% of the molten mantle. Although the SMO is kept molten through the intense stellar flux, there is no considerable vertical conduction or convection.

3 Methodology

This thesis will consider only the end-member cases, Stage 1 and Stage 4. Although Stage 2 and Stage 3 could be long periods, studying the end-member cases gives us the limit behaviors of the atmospheres and all plausible atmospheric dynamics for Stage 2 and 3 will be within these limits. The methodology for calculating opacity and flux absorption by the atmosphere is described below. Note that I used Python as my programming language for all the calculations described in this thesis.

Firstly, the surface temperature T_{surf} is calculated through radiative equilibrium as a function of co-latitude θ (see Section 2.5 for exact method). Secondly, partial vapor pressures $P_i(T_{\text{surf}})$ for different atmospheric species $i \in \mathcal{A}$ are needed. Input data files from Dr. Boukaré and Dr. Nguyen containing magma ocean compositions are fed to LavAtmos (see Section 3.1), resulting in 2 files containing temperature-dependent saturated partial pressure values: one corresponding to Stage 1 and the other to Stage 4. These .txt files given to me by Dr. Nguyen will finally be used to calculate the radiative absorption of the atmosphere.

The first row of the files consists of a list of surface temperatures. The rest of the rows contain elements of the type $\log_{10}(P_i)$, where each row corresponds to the partial vapor pressure (T_{surf} dependent) values of a specific atmospheric species. To have a readily accessible $P_i(T_{\text{surf}})$ function, a polynomial fit is used. As $T_{\text{surf}}(\theta)$ and $P_i(T_{\text{surf}})$ are known $\forall i \in \mathcal{A}$, $P_i(\theta)$ can be easily calculated, as well as the total pressure of the atmosphere $P_t(\theta) = \sum_{i\in\mathcal{A}} P_i(\theta)$.

Now total opacity $\epsilon(\lambda, \theta)$ can be calculated. The needed absorption cross-section $x_i(\lambda, P_t, T_{\text{surf}})$ is obtained for each species $i \in \mathcal{A}$ from ExoMol (read Section 3.2). Clearly, x_i depends on a pressure value and a temperature value. In our case, it will be the total pressure of the atmosphere and the surface temperature. As both depend on θ, we now have $x_i(\lambda, \theta)$. Total opacity $\epsilon(\lambda, \theta)$ as well as individual opacities $\epsilon_i(\lambda, \theta)$ can then be calculated using Eq (3) and Eq (4). The stellar flux $F_{\text{stel}}(\theta)$ and $F_{\text{surf}}(\theta)$ are calculated using Eq (5) and Eq (6), and broadband opacity $\epsilon_B(\theta)$ through Eq (8).

3.1 LavAtmos

LavAtmos is a publicly-available code that takes surface temperature and magma melt composition as inputs and outputs the equilibrium partial vapor pressures of the atmospheric species just above the magma melt (Buchem et al. 2023). Atmospheric models like this one are necessary because they handle complex geochemistry in the atmosphere, which is required for characterizing its composition via JWST's spectroscopic measurements. LavAtmos bridges the chemistry between the magma ocean and mineral-vapor atmosphere, and can help us understand what type of atmospheric compositions we should expect.

3.2 ExoMol

To retrieve the absorption cross-section data for the atmospheric species in $\mathcal{A}$, I used the ExoMol website. ExoMol is an open and accessible database with molecular information about different atmospheric species designed for use in simulation and characterization of exoplanet atmospheres (Tennyson et al. 2016). For more information about ExoMol, see Appendix 6.3.

4 Results

This section presents the results of this thesis. First, atmospheric and surface conditions will be explored for both stages. Then, the atmospheric optical properties will be discussed, followed by the final analysis of the radiative transfer of K2-141b's atmosphere.

Note that only radiative transfer is considered for the results of this thesis. Hydrodynamics may change how the atmosphere interacts with the surface as well as keeping the atmosphere not radiatively balanced; implementing all the dynamics into a general model is still in development.

4.1 Atmospheric and surface conditions

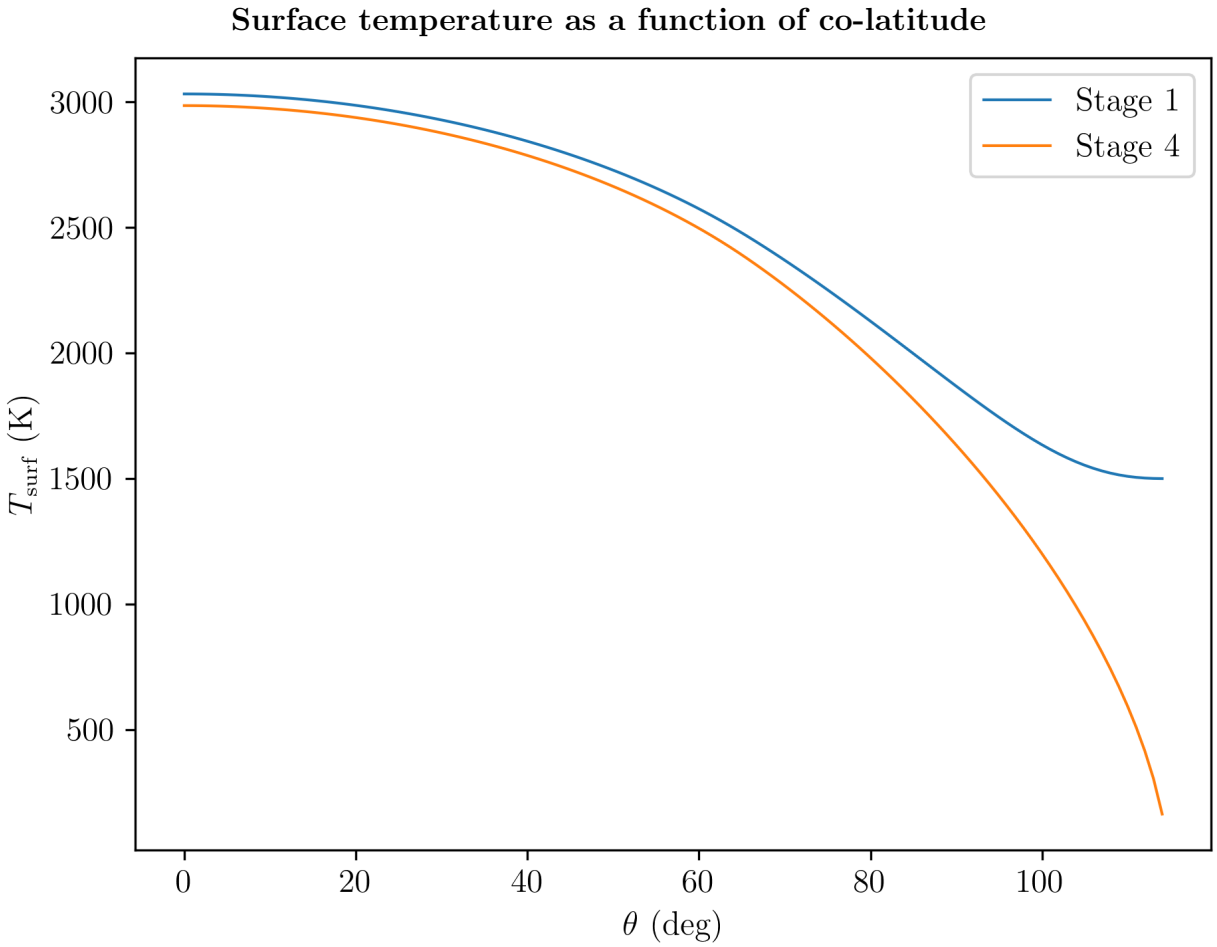

Figure 1: Surface temperature for different stages of lava planet K2-141b. Substellar temperature is 3032 K for Stage 1 and 2986 K for Stage 4.

The evolution of surface temperatures for different stages is shown in Figure 1. In Stage 1, the geothermal flux from the deep magma ocean leads to a higher surface temperature in all co-latitudes, with a substellar temperature of 3032 K. This is expected, as convection from the deep mantle of the GMO will supply more heat to the surface than convection from a SMO. As co-latitude approaches $\theta \approx 115°$, the temperatures plateaus into 1500 K, which is the average nightside temperature.

In Stage 4, geothermal flux is negligible, and the surface temperatures are primarily shaped by stellar irradiation. Specifically, surface temperatures drop from 2986 K in the substellar

point to 100 K on the nightside. In addition, there is a greater temperature gradient with respect to angular distance when compared to Stage 1, especially near the terminator. The surface cools way faster during Stage 4 due to the significantly reduced geothermal heating and the lower efficiency of heat redistribution in a SMO compared to a GMO.

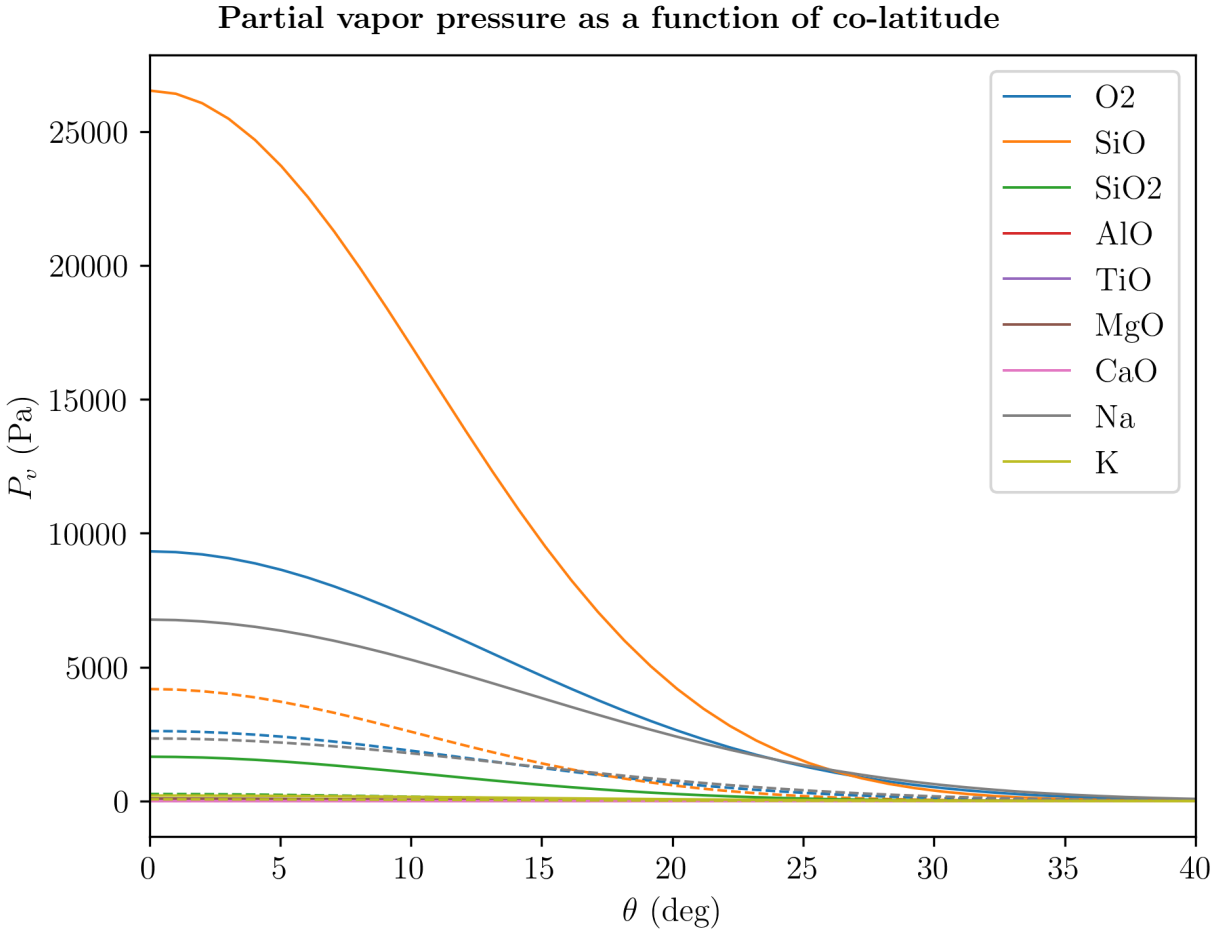

Figure 2: Partial vapor pressures of species in $\mathcal{A}$ right above K2-141b's surface. Solid lines represent Stage 1 and dashed lines represent Stage 4.

Surface temperature has a big influence on outgassing processes in K2-141b, as partial vapor pressures have an exponential relation with temperature (see Figure 2). Figure 2 is only plotted up to $\theta = 40°$, as partial pressures become vanishingly small after that point. Consequently, this is an indicator that the bulk of the atmosphere might be located near the substellar point in both stages and might not uniformly cover all of the dayside. However, there could still be a thinner and tenuous fluid layer for larger co-latitudes (Nguyen, Cowan, Banerjee, et al. 2020).

In addition, the dashed lines show how an atmosphere in Stage 4 is less dense and more localized than the atmosphere in Stage 1. All of the component's vapor partial pressures decrease considerably from Stage 1 to Stage 4. This difference arises from the variation in geothermal heating: if the same geothermal heat is assumed for both stages, partial pressure values are virtually indistinguishable in both stages[2]. This indicates that the evolution of ocean composition does not have a significant effect on the atmosphere, but the change in interior heating, and consequently surface temperatures, does.

[2]If the same surface temperature is assumed for both stages, the solid and dashed lines in Figure 1 would overlap. The maximum relative difference I calculated is only 0.2 %.

Cloud formation is a possibility in lava planets like K2-141b (Nguyen, Cowan, and Dang 2024). However, because the atmosphere in Stage 4 collapses at smaller co-latitudes, cloud formation is expected to behave differently across evolutionary stages. The denser atmosphere in Stage 1 favors a higher global condensation rate, while the more localized atmosphere and fast surface cooling in Stage 4 may lead to condensation that is closer to the substellar point.

The main components that stand out (in both stages) are SiO, O_2, Na and SiO_2. This result is consistent with literature, as these four atmospheric species are expected to be common in a lava planet's atmosphere (Zilinskas et al. 2022). Silicates SiO and SiO_2 being dominant constituents is due to the overwhelming abundance of silicon oxides found in the rocky mantle of K2-141b. Na is also dominant because it is a highly volatile material and has low vaporization temperature (Schaefer, Lodders, and Fegley Jr. 2012). It also has a big impact on optical depth as Figure 3 shows. As for O_2, it could come from the dissociation of metal oxides as they vaporize (like SiO_2, FeO, Fe_2O_3 and other common species in magma).

If the atmosphere is purely constrained to ocean dynamics, the atmospheric abundances of Na and K are not depleted by Stage 4. This is because the magma ocean itself has no mechanism for Na and K depletion. They are very easy to keep molten and do not sink to the core, as seen in Table 2. In Figure 2, we are only treating atmospheric dynamics as a reaction to changes in the magma ocean. To account for the depletion of volatile and light material, we assess the consequences of cold-trapping and atmospheric escape in Section 4.3.2.

4.2 Optical properties of the atmosphere

Although Figure 3 is only specific to Stage 1, it should give the reader an overview of the general spectroscopic trends of a lava planet atmosphere's optical properties. Figure 4 compares total opacities of the different stages at the substellar point, along with other values for surface temperatures (in Stage 1). A logarithmic scale was used for both figures because wavelength spans over several orders of magnitude and a linear scale would not have allowed to see clearly lower values and higher values at the same time.

Figure 3 shows the optical depth of the 9 available species in ExoMol with the substellar point temperature. At the substellar point, the main contributors to the optical depth are MgO, SiO, K and Na. For the UV range, the main dominant contributors are Na, K and SiO. During the visible range these species continue to dominate, especially Na, with its famous doublet. Also, MgO starts to dominate in the visible [3].

During the IR range, oxides start to contribute more, with SiO having an important spectral line at 9 μm that is expected to be a good parameter for observation in lava planet spectroscopy with JWST (Nguyen, Cowan, Pierrehumbert, et al. 2022). SiO_2 and MgO also play an important role in the IR region. Although MgO is not very abundant in the atmosphere because of its high melting temperature (as seen in Figure 2), it is still important because of its large absorption cross-section per molecule across visible and IR wavelengths. Overall, Figure 3 supports the claim that volatiles tend to dominate in the UV/visible wavelengths while refractory species dominate the IR (Zilinskas et al. 2022).

[3] UV range: 0.1 - 0.4 μm, Visible range: 0.4 - 0.7 μm and IR range: from 0.7 μm

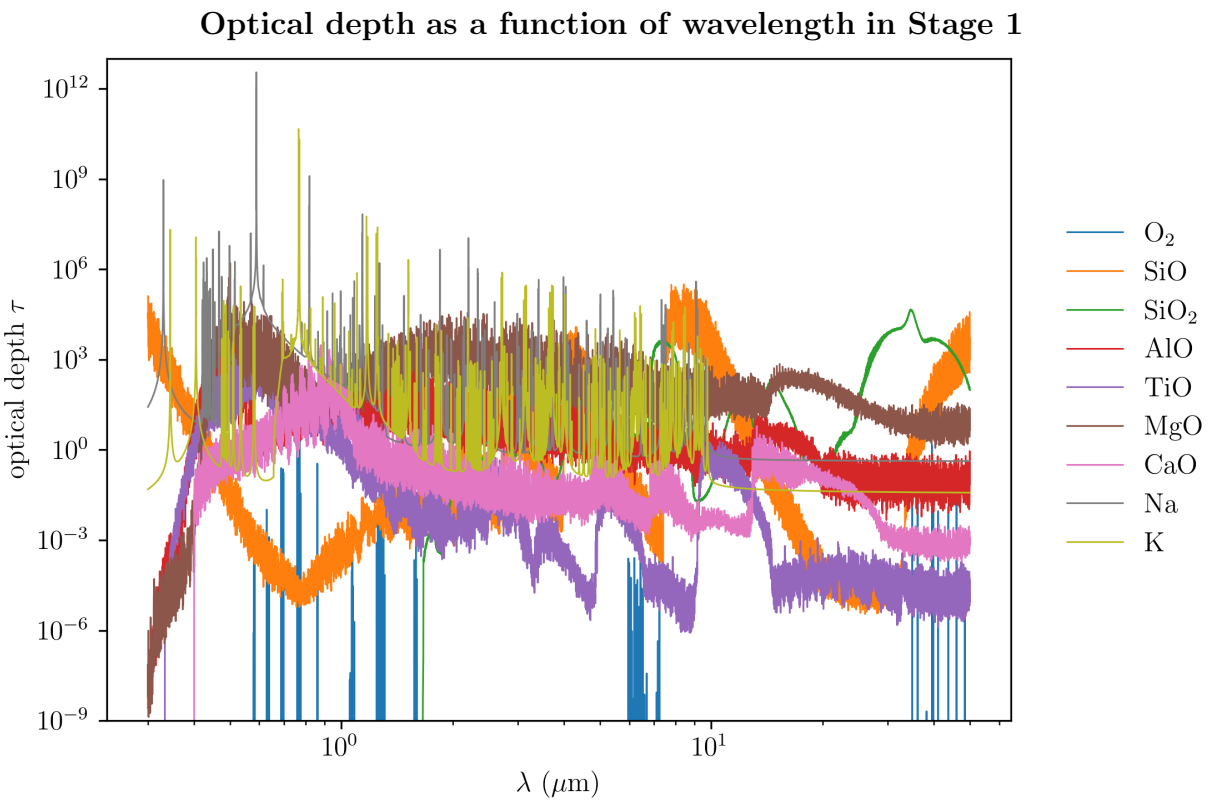

Figure 3: Optical depth of all the available species in ExoMol as a function of wavelength in Stage 1 calculated with Eq (4). The surface temperature used for this plot is the substellar equilibrium temperature $T = 3032$ K. The total pressure is 44595,83 Pa. The λ axis is set on a logarithmic scale.

Figure 4 shows the total opacity for different surface temperatures (and in different stages), which in turn correspond to different co-latitudes in K2-141b. As the temperature decreases, the total opacity decreases too. For a substellar temperature of $T = 3032$ K in Stage 1, opacity is 1 across the spectrum. This implies that the atmosphere around the substellar point in Stage 1 is completely opaque. When doing the same for Stage 4, there are significant opacity windows in the IR. As a result, the atmosphere near the substellar point is generally less opaque in Stage 4 than the atmosphere of Stage 1. Because the surface is cooler in Stage 4 and therefore outgasses much less material in all co-latitudes, the physically thin atmosphere of Stage 4 is expectedly much more optically thin than in Stage 1. The difference is even bigger when atmospheric escape and cold-trapping are considered.

As Figure 4 shows, the opacity in both stages is primarily controlled by the surface temperature. As surface temperature decreases, the total opacity drops drastically, and between 2000 K and 1800 K the only noticeable absorption features are the sodium doublet (see Appendix 6.4 for further details). Hence, an opaque atmosphere near the substellar point can quickly transition into an optically thin atmosphere as co-latitude increases. For surface temperatures under 1800 K, the opacity is basically 0.

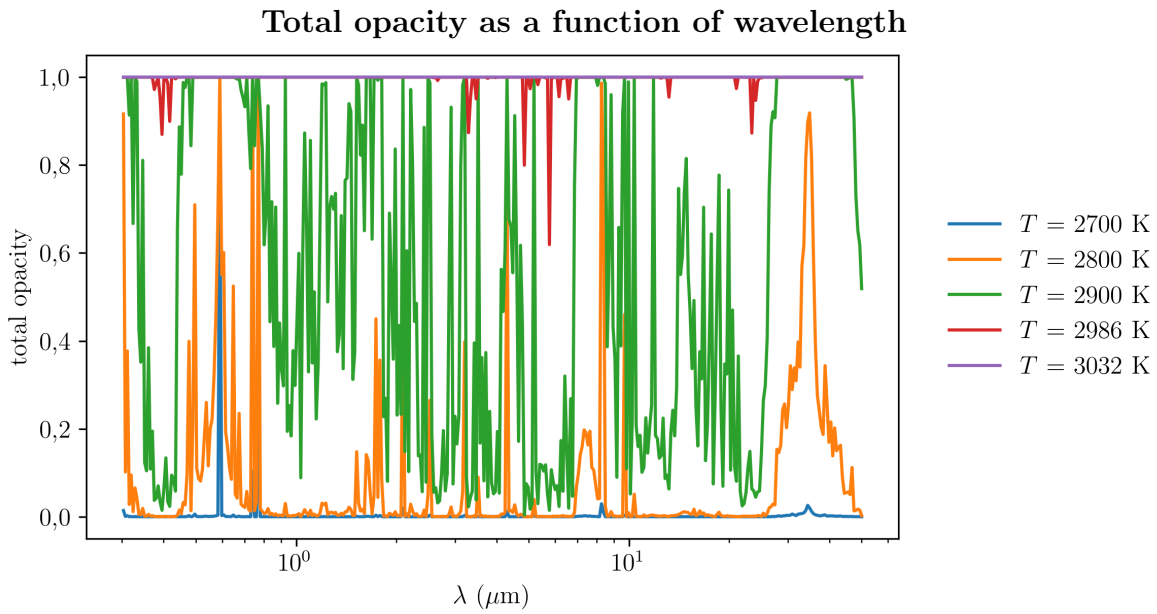

Figure 4: Total opacity of the atmosphere at different temperatures. $T = 3032$ K corresponds to the substellar temperature in Stage 1 while $T = 2986$ K corresponds to the substellar temperature in Stage 4. For temperatures 2700, 2800 and 2900 K the atmospheric composition of Stage 1 was used. Surface temperatures have a bigger influence on the atmosphere than magma ocean composition, which is why for these last three temperatures it did not matter which stage was chosen.

4.3 Radiative transfer analysis of K2-141b's atmosphere

This section will first explore how much stellar and surface flux is absorbed by the atmosphere in different stages. Secondly, it will assess the effects of cold-trapping in the radiative transfer of the atmosphere in Stage 4. Finally, broadband opacity will be discussed to obtain conclusions about K2-141b's observability.

4.3.1 Analysis of stellar and surface flux absorption in Stage 1 and Stage 4

Figure 5 shows that both the surface and stellar flux absorbed by the atmosphere near the substellar point have an order of magnitude of 10^6 W/m^2 in both stages, which is 10 times higher than geothermal flux in Stage 1. In comparison, Earth receives 1360 W/m^2 of solar flux, of which only about one quarter is actually absorbed by the atmosphere (K. Wang, P. Wang, and Sparrow 2014). In K2-141b's case, it is 3 orders of magnitude higher, explaining the high surface temperatures and the magma ocean.

However, as co-latitude reaches $\theta \approx 50°$, the stellar and surface fluxes in both stages decrease to near 0 values. This is due to the diminishing opacity and surface temperature decline (as seen in Figure 4). After $\theta \approx 50°$, the atmosphere is both physically and optically thin, and dynamics are no longer dominated by radiative transfer but by mechanical processes caused by atmospheric flow.

When comparing stages, Figure 5 shows that more total flux is absorbed during Stage 1. Although a higher total absorbed flux could indicate higher atmospheric temperatures in Stage 1, no radiative cooling calculations have been performed in this thesis, and therefore, no definitive conclusions can be made regarding absolute atmospheric temperatures. However, the relative contribution of the stellar flux and the surface flux can be taken into account to make a qualitative analysis about the potential vertical thermal structure of the atmosphere.

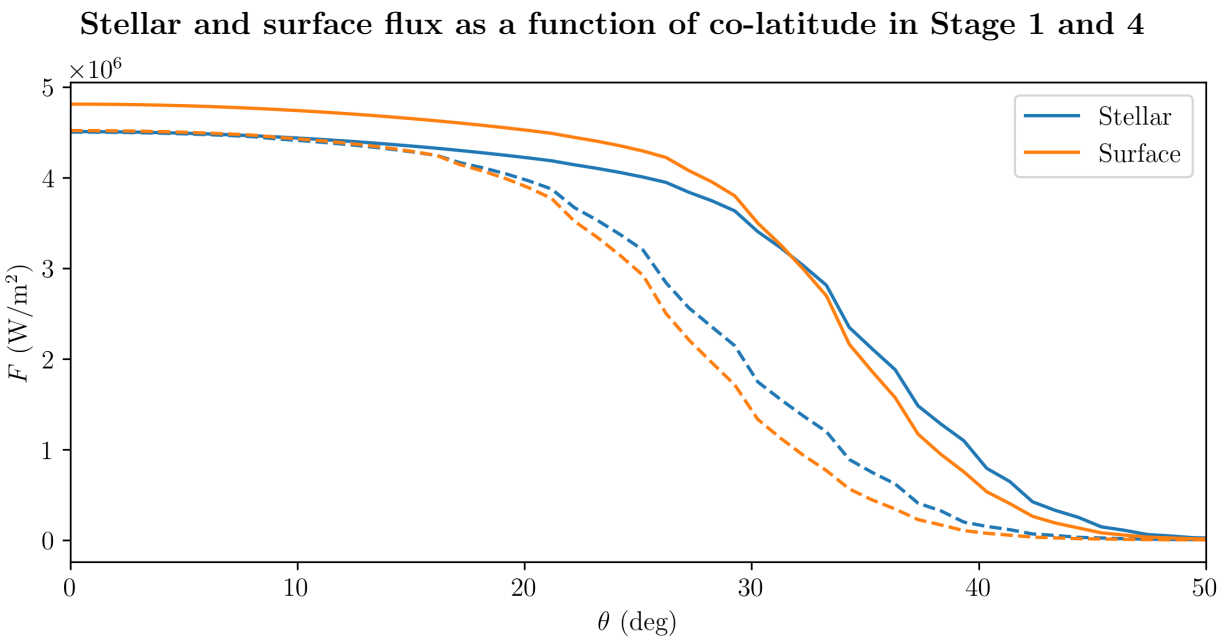

Figure 5: Stellar and surface flux absorbed by K2-141b's atmosphere for different co-latitudes. Solid lines represent Stage 1 and dashed lines represent Stage 4.

In Stage 1, surface flux begins at a higher value than stellar flux. This is due to the surface blackbody emission coming from significant geothermal flux on top of the incident stellar flux that made it to the surface. For $\theta < 33°$, as surface flux is higher than stellar flux, atmospheric temperature decreases with altitude, making the top layer of the atmosphere the coldest. As co-latitudes increase, the gap between stellar and surface flux decreases until eventually stellar flux overtakes surface flux as the main contributor, mainly caused by the decrease in surface temperature shown in Figure 1.

When stellar flux is higher than surface flux, the top of the atmosphere is hotter than the bottom of the atmosphere because heat is deposited more from the top than from the bottom of the atmosphere. This can cause thermal inversions, which are well documented for lava planets (Zieba et al. 2022). Figure 5 predicts a thermal inversion layer only after $\theta \approx 33°$ (in Stage 1).

In Stage 4, represented by the dashed lines in Figure 5, surface flux and stellar flux absorbed by the atmosphere is the same for small values of θ. This is due to the opacity being close to 1 (atmosphere optically thick) near the substellar point and a negligible geothermal flux. With negligible geothermal forcing, surface flux and stellar flux absorption in the atmosphere is similar as a consequence of surface radiative balance and $\epsilon = 1$ [4]. For co-latitudes under $\theta \approx 16°$, a vertically isothermal temperature is favored, as the atmosphere is receiving the same amount from the top than the bottom. For co-latitudes bigger than $\theta \approx 16°$, stellar flux begins to dominate the atmosphere, causing thermal inversions to be plausible.

[4]Essentially, all of the absorbed stellar flux is then re-emitted to the surface. When $\epsilon \approx 1$, the atmosphere acts as if it was a rock layer on top of the mantle.

4.3.2 Modeling cold-trapping in Stage 4

Figure 5 displays the radiative transfer analysis for Stage 4, assuming no cold-trapping on the nightside of volatile species like Na and K. Although our initial calculations did not include cold-trapping and only focused on magma ocean dynamics and composition, volatiles like Na and K are likely to be depleted by Stage 4 (Ito and Ikoma 2021). To explore the effects of cold-trapping, this section compares a Stage 4 atmosphere with and without these volatiles, as shown in Figure 6.

For low co-latitudes where opacity is close to 1, there is no visible difference between the solid and the dashed lines up to $\theta \approx 15°$. This indicates that in this saturated region, the subtraction of Na and K will not affect the overall opacity in a considerable way. However, for higher co-latitudes, both stellar and surface flux absorbed by the atmosphere in Stage 4 are lower if Na and K are missing. This is because Na and K maintain a high optical depth (due to their high volatility and large absorption cross-section in visible wavelengths) even when the atmosphere becomes thinner for bigger co-latitudes.

Without Na and K, the atmosphere is significantly more optically thin, leading to less absorbed flux in the atmosphere as seen in Figure 6. In addition, volatile depletion favors a vertically isothermal temperature profile over a thermal inversion as the dashed lines in Figure 6 are closer to each other than the solid lines.

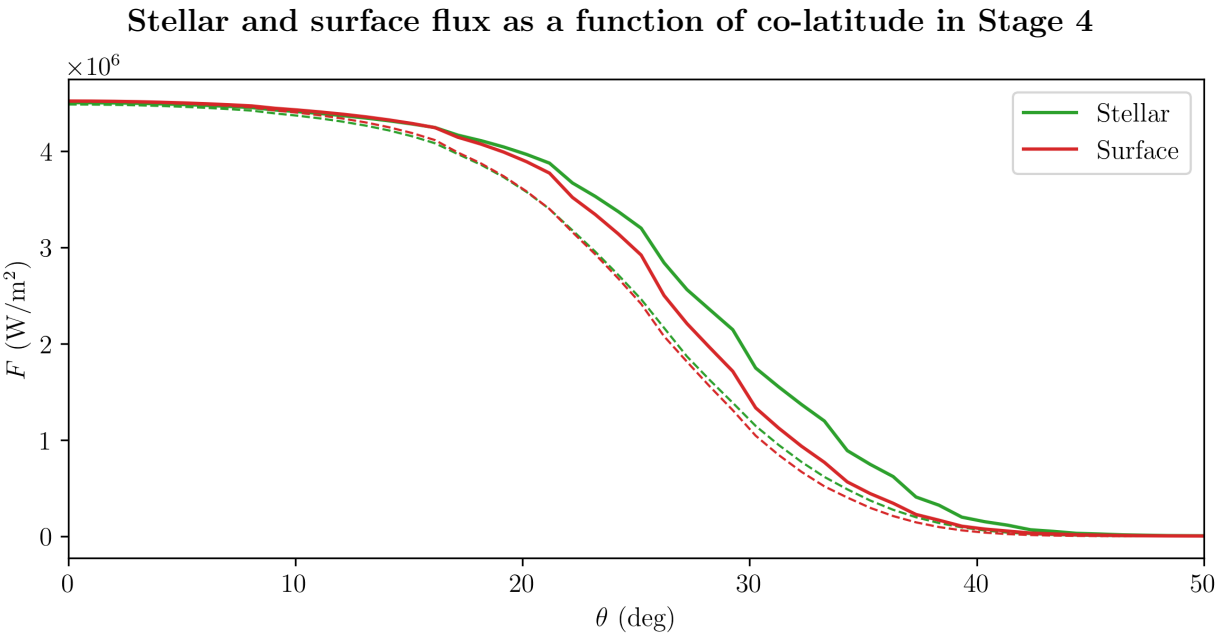

Figure 6: Stellar and surface flux absorbed by the atmosphere at different co-latitudes. Solid lines represent Stage 4 with all species in $\mathcal{A}$ and dashed lines represent Stage 4 with species $\mathcal{A}\backslash\{\text{Na,K}\}$. The solid lines in this plot correspond to the dashed lines in Figure 5.

4.3.3 Broadband opacity

Figure 7 shows the different broadband opacities for Stage 1, Stage 4, and Stage 4 without volatiles. Physically, ϵ_B represents the fraction of stellar flux absorbed by the atmosphere in comparison to the total stellar flux reaching the planet's atmosphere. Because ϵ_B is weighted against the stellar spectrum, it is biased towards visible wavelengths as most star light is visible light.

At small co-latitudes $\theta \approx 5°$, the three scenarios described above have opacities all close to 1. In this region near the substellar point, the atmosphere is very opaque and saturated, making it difficult to distinguish the differences. This is consistent with Figure 5 and Figure 6, where stellar fluxes show similar initial conditions for low co-latitudes. The depletion of volatiles causes negligible effects in this region because the atmosphere is already saturated without these volatiles.

In the intermediate region $\theta \in [5, 50]°$, all three broadband opacities start decreasing drastically but at different rates. As Figure 7 shows, a Stage 1 atmosphere would absorb more stellar flux than a Stage 4 atmosphere. If Na and K were excluded in this Stage 4 atmosphere, it would become even less opaque. After $\theta \approx 50°$, broadband opacities come close to 0, implying an optically thin atmosphere from that point in the three different atmospheres.

For observability purposes, $\theta \in [5, 50]°$ is the region of K2-141b that will likely give the best observational data. For smaller co-latitudes, opacity is close to 1, and all of the stellar flux is absorbed by the atmosphere, leaving our telescopes unable to observe the transmitted flux. If opacity is close to 0, then the stellar flux will just go right through and no atmospheric species will be detected.

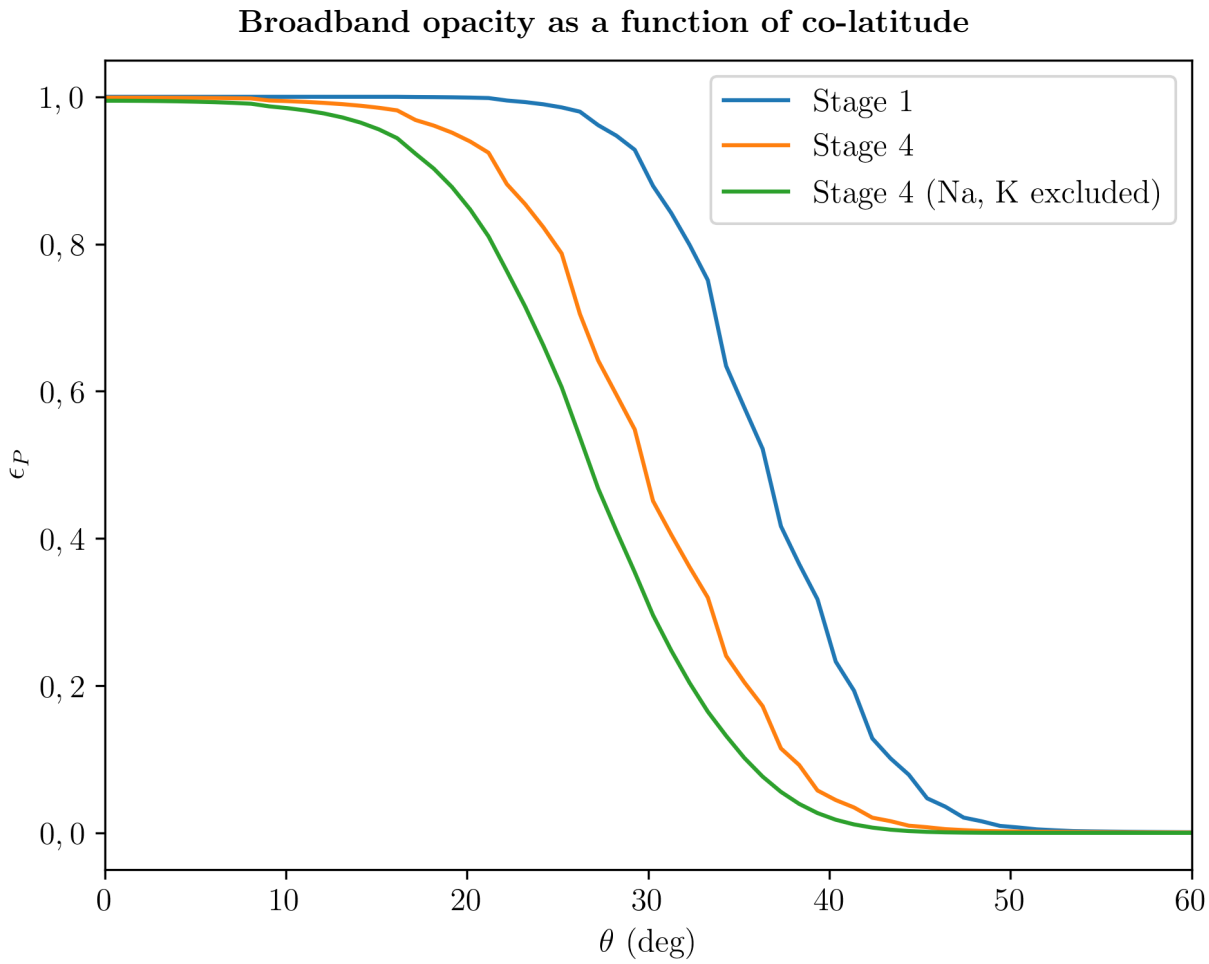

Figure 7: Broadband opacity as a function of co-latitude for Stage 1, Stage 4 and Stage 4 without Na and K.

5 Conclusions

The objectives of this thesis have been achieved. I have developed a Python framework to calculate the total opacity and compute the absorbed stellar and surface flux for any given atmospheric composition. In addition, a radiative transfer analysis of K2-141b's atmosphere has been performed with this framework. These results and tools will help Dr. Nguyen with his ongoing development of a coupled hydrodynamics and radiative transfer model for exoplanet atmospheres.

The initial hypothesis has been partially confirmed: while changes in the magma ocean composition do not significantly affect the atmosphere, ocean dynamics play a central role. The geothermal flux of the molten mantle in Stage 1 forces surface temperatures across all co-latitudes to be higher compared to Stage 4. Consequently, the atmosphere in Stage 1 is denser, optically thicker, and more extended throughout K2-141b, while the Stage 4 atmosphere is optically thinner, has lower atmospheric pressure, and is more localized to the substellar point. As predicted, the atmosphere absorbs more total flux during Stage 1.

For observability purposes, the best conditions for detecting spectral features and characterizing K2-141b's atmosphere are found in the volatile-free Stage 4 scenario. Since this is the evolutionary state K2-141b is currently believed to be in, upcoming observational data from JWST may soon provide valuable insights.

In this thesis, the limitations reside in the number of assumptions taken and the fact that the atmosphere is modeled as a response to ocean dynamics. For future work, a hydrodynamical model needs to be used jointly with a radiative transfer model, taking magma ocean and atmosphere self-consistent coupling into account. This model would also enable radiative cooling calculations, which are needed for a full radiative transfer analysis of an atmosphere. The development of such models will help us understand the observations of K2-141b by JWST and other lava planets that may be observed in the future.

6 Exhibits

6.1 Molar masses

Obtained from the National Institute of Standards and Technology (NIST) 2024.

Table 3: Molar masses of species in $\mathcal{A}$

Species	**Molar mass (g/mol)**
SiO	44,0845
SiO_2	60,0843
Na	22,9898
O_2	31,998
AlO	42,9802
TiO	63,865
MgO	40,3044
CaO	56,0774
K	39,0983

6.2 Formulas for dayside surface temperature calculation

The uncertainty formulas for θ_f and θ_d are given in rad, they need to be multiplied by $180/\pi$ to obtain the uncertainty in degrees.

- Uncertainty for θ_f

$$u_{\theta_f} = \frac{1}{d\sqrt{1-\left(\frac{R_p+R_*}{d}\right)^2}}\sqrt{u_{R_p}^2 + u_{R_*}^2 + \left(\frac{R_p+R_*}{d}\right)^2 u_d^2}. \tag{13}$$

- Uncertainty for θ_d

$$u_{\theta_d} = \frac{1}{d\sqrt{1-\left(\frac{R_p-R_*}{d}\right)^2}}\sqrt{u_{R_p}^2 + u_{R_*}^2 + \left(\frac{R_p-R_*}{d}\right)^2 u_d^2}. \tag{14}$$

Note that the following two formulas are extracted from Appendix A in (Kang, Nimmo, and Ding 2023). In the fully illuminated region, the geometrical factor $J_f(\theta)$ is

$$J_f(\theta) = \left(\frac{(d\cos\theta - R_p)R_*^2}{\rho(\theta)^3}\right), \tag{15}$$

where $\rho = \sqrt{d^2 + R_p^2 - 2dR_p\cos\theta}$. In the penumbria region, the geometrical factor $J_p(\theta)$ is

$$J_p(\theta) = \left(\frac{\sin^2\phi\cos\alpha}{\pi}[\pi - \delta_2 + \sin\delta_2\cos\delta_2] + \frac{1}{\pi}[\delta_1 - \sin\delta_1\cos\delta_1]\right), \tag{16}$$

where $\phi, \alpha, \delta_1, \delta_2$ are angles arising from the specific geometrical configuration. For more information on how these formulas are obtained and what each angle represents, see Apendix A in (Kang, Nimmo, and Ding 2023).

6.3 TauREx package keys

TauREx files are a type of file found in ExoMol that contain absorption cross-sections of different atmospheric species. The package keys of a TauREx file are found in Figure 8:

Field name	Description
mol_name	Molecule name
key_iso_ll	ID for isotopologue and line list
t	List of temperatures
p	List of pressures
t.units	Units of temperature (K)
p.units	Units of pressure (bar)
bin_edges	Bin edges in wavenumbers (cm^{-1})
bin_edges.units	Units of bin edges (cm^{-1})
xsecarr	Cross-section array (*p*, *t*, *bin_centres*)
xsecarr.units	Cross-section units, cm^2/molecule
mol_mass	Molecular mass in a.m.u.
DOI	Digital Online Identifier for line list
Date_ID	ID for date of creation and version

Figure 8: TauREx package keys

6.4 Total opacity and surface temperature

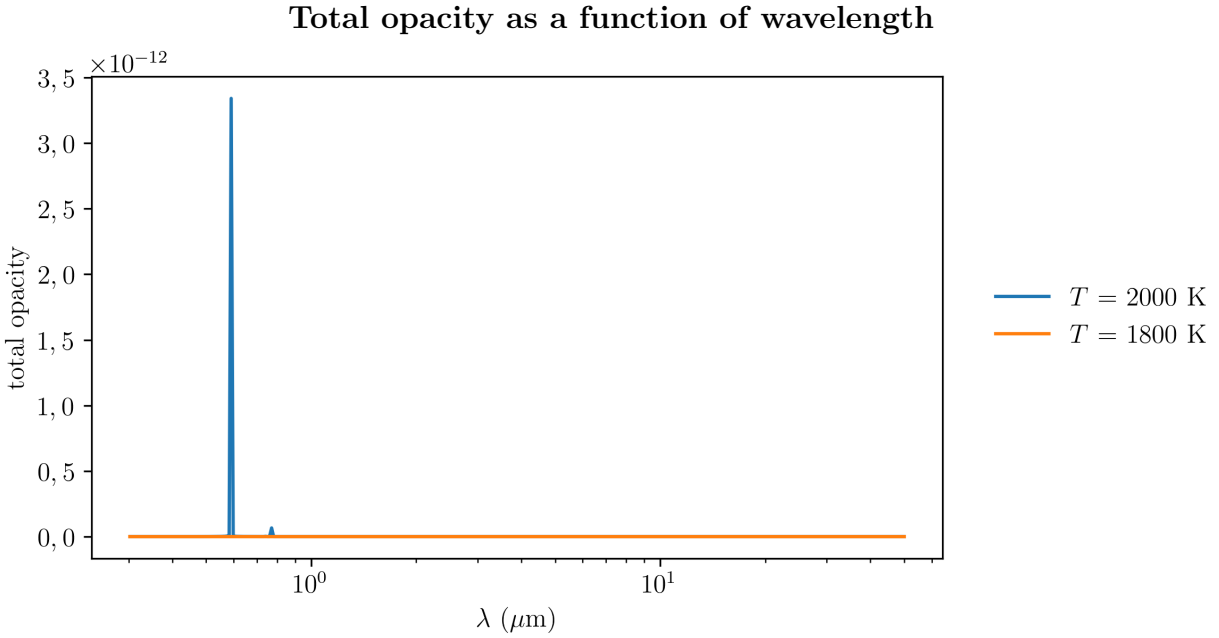

Figure 9: Total opacity in 2000 K and 1800 K for Stage 1

In Stage 1, only the sodium doublet remains at $T = 2000$ K. At $T = 1800$ K, the total opacity of K2-141b's atmosphere is negligible.

References

Bonomo, A. S. et al. (2023). "Cold Jupiters and improved masses in 38 Kepler and K2 small planet systems from 3661 HARPS-N radial velocities". In: *Astronomy & Astrophysics* 677. Published online 29 August 2023, A33. DOI: 10.1051/0004-6361/202346211.

Boukaré, C.-É. et al. (2023). *Lava planets interior dynamics govern the long-term evolution of their magma oceans*. arXiv: 2308.13614 [astro-ph.EP]. URL: https://arxiv.org/abs/2308.13614.

Buchem, C. P. A. van et al. (July 2023). "LavAtmos: An open-source chemical equilibrium vaporization code for lava worlds". In: *Meteoritics amp; Planetary Science* 58.8, pp. 1149–1161. ISSN: 1945-5100. DOI: 10.1111/maps.13994. URL: http://dx.doi.org/10.1111/maps.13994.

Herath, D. et al. (2024). "Thermal evolution of lava planets". In: *Monthly Notices of the Royal Astronomical Society* 535.3, pp. 2404–2418. DOI: 10.1093/mnras/stad1234. URL: https://academic.oup.com/mnras/article/535/3/2404/7849768.

Ito, Y. and M. Ikoma (2021). "Theoretical thermal evolution of close-in rocky exoplanets: importance of atmospheric blanketing effect on magma ocean solidification". In: *The Astrophysical Journal* 916.1, p. 24. DOI: 10.3847/1538-4357/ac02b1.

Kang, W., F. Nimmo, and F. Ding (2023). *True Polar Wander of Lava Worlds*. arXiv: 2306.06768 [astro-ph.EP]. URL: https://arxiv.org/abs/2306.06768.

Kaushik, M., A. Mattoo, and R. Rastogi (2024). *Exoplanet Detection : A Detailed Analysis*. arXiv: 2404.09143 [astro-ph.EP]. URL: https://arxiv.org/abs/2404.09143.

Kite, E. S. et al. (2016). "Atmosphere-Interior Exchange on Hot Rocky Exoplanets". In: *The Astrophysical Journal* 828.2, p. 80. DOI: 10.3847/0004-637X/828/2/80.

Kopal, Z. (1954). "Photometric Effects of Reflection in Close Binary Systems". In: *Monthly Notices of the Royal Astronomical Society* 114.1, pp. 101–117. DOI: 10.1093/mnras/114.1.101. URL: https://academic.oup.com/mnras/article/114/1/101/2602045.

Kracek, F. C. (1963). *Melting and Transformation Temperatures of Mineral and Allied Substances*. Vol. 1144-D. U.S. Geological Survey Bulletin. Part of the "Data of Geochemistry" series. Accessed May 2025. Washington, D.C.: U.S. Government Printing Office. URL: https://pubs.usgs.gov/bul/1144d/report.pdf.

Malavolta, L. et al. (Feb. 2018). "An Ultra-short Period Rocky Super-Earth with a Secondary Eclipse and a Neptune-like Companion around K2-141". In: *The Astronomical Journal* 155.3, p. 107. DOI: 10.3847/1538-3881/aaa5b5. URL: https://dx.doi.org/10.3847/1538-3881/aaa5b5.

National Institute of Standards and Technology (NIST) (2024). *NIST Chemistry WebBook*. URL: https://webbook.nist.gov/chemistry/.

Nguyen, T. G., N. B. Cowan, A. Banerjee, et al. (Nov. 2020). "Modelling the atmosphere of lava planet K2-141b: implications for low- and high-resolution spectroscopy". In: *Monthly Notices of the Royal Astronomical Society* 499.4, pp. 4605–4612. ISSN: 1365-2966. DOI: 10.1093/mnras/staa2487. URL: http://dx.doi.org/10.1093/mnras/staa2487.

Nguyen, T. G., N. B. Cowan, R. T. Pierrehumbert, et al. (May 2022). "The impact of ultraviolet heating and cooling on the dynamics and observability of lava planet atmospheres". In: *Monthly Notices of the Royal Astronomical Society* 513.4, pp. 6125–6133. ISSN: 1365-2966. DOI: 10.1093/mnras/stac1331. URL: http://dx.doi.org/10.1093/mnras/stac1331.

Nguyen, T. G., N. B. Cowan, and L. Dang (2024). *Clouds on partial atmospheres of lava planets and where to find them*. arXiv: 2407.21111 [astro-ph.EP]. URL: https://arxiv.org/abs/2407.21111.

Schaefer, L. and L. T. Elkins-Tanton (2018). "Magma oceans as a critical stage in the tectonic development of rocky planets". In: *Philosophical Transactions of the Royal Society A: Mathematical, Physical and Engineering Sciences* 376.2132, p. 20180109. DOI: 10.1098/rsta.2018.0109.

Schaefer, L., K. Lodders, and B. Fegley Jr. (2012). "Vaporization of the Earth: Application to Exoplanet Atmospheres". In: *The Astrophysical Journal* 755.1, p. 41. DOI: 10.1088/0004-637X/755/1/41.

Tennyson, J. et al. (2016). "The ExoMol database: molecular line lists for exoplanet and other hot atmospheres". In: *Journal of Molecular Spectroscopy* 327, pp. 73–94. DOI: 10.1016/j.jms.2016.05.002. URL: https://www.sciencedirect.com/science/article/pii/S0022285216300807.

Wang, K., P. Wang, and M. Sparrow (2014). "Global atmospheric downward longwave radiation over land surface under all-sky conditions from 1973 to 2008". In: *Journal of Climate* 27.5, pp. 1651–1661. DOI: 10.1175/JCLI-D-13-00335.1.

Zieba, S. et al. (Aug. 2022). "K2 and Spitzer phase curves of the rocky ultra-short-period planet K2-141 b hint at a tenuous rock vapor atmosphere". In: *Astronomy amp; Astrophysics* 664, A79. ISSN: 1432-0746. DOI: 10.1051/0004-6361/202142912. URL: http://dx.doi.org/10.1051/0004-6361/202142912.

Zilinskas, M. et al. (May 2022). "Observability of evaporating lava worlds". In: *Astronomy amp; Astrophysics* 661, A126. ISSN: 1432-0746. DOI: 10.1051/0004-6361/202142984. URL: http://dx.doi.org/10.1051/0004-6361/202142984.